Negative Stiffness Materials for Vibration Damping: a Material Realization of a Nonlinear Bistable Element

Jan Heczko[1], Zuzana Dimitrovová*[2], Hélder C. Rodrigues[3]

[1]Department of Mechanics, Faculty of Applied Sciences, University of West Bohemia, Pilsen
[2]Departamento de Engenharia Civil, Faculdade de Ciências e Tecnologia, Universidade Nova de Lisboa and LAETA, IDMEC, Instituto Superior Técnico, Universidade de Lisboa, Lisboa, Portugal
[3]LAETA, IDMEC, Instituto Superior Técnico, Universidade de Lisboa, Lisboa, Portugal
* zdim@fct.unl.pt

Abstract— This paper addresses material and shape design of a prototype exhibiting a negative stiffness over a finite range of global strains. The objective is to define a design loop, where, starting from the actual material realization, a corresponding finite element model is developed and associated to a bistable discrete one-dimensional mechanical system composed of pre-compressed springs, a stabilizing spring and a damper. The discrete model can easily be analyzed and optimized for improved vibration damping properties. This will allow the determination of an alternative specification of a new optimized prototype. If confirmed by finite element analysis, then an improved prototype can be produced accordingly. This paper presents the first results: the material realization and the corresponding discrete model identification exploring also the finite element model. Optimization will be subject of further research. It is concluded that the specimen behaves according to the expectations, i.e. the negative stiffness region is well-formed and the discrete correspondence is easily obtainable. Such a structure can be used as a negative-stiffness element to achieve extreme mechanical properties of a composite or as a structure with improved damping properties.

Keywords—**Experimental Testing, Finite Element Modelling, Negative Stiffness, Nonlinear Bistable Element, Vibration control.**

I. Introduction

RECENT PROGRESS in material processing and manufacturing has stimulated strong scientific and industrial interest in material design optimization. Tailoring material properties to achieve the optimal response to a given solicitation provides an important input to the development of new materials. New horizons in novel materials can be opened if the concept of the structural negative stiffness is considered.

Materials with adequate mixtures of carefully selected phases, including also a negative stiffness phase, have been shown to possess the ability of reaching extreme properties, such as stiffness or vibration damping [1, 2]. Apart from many studies exploring theoretically advances achieved in materials incorporating negative stiffness constituents [3] there are also real world applications that had proven utility of this concept. Attempts to manufacture such materials were made using unstable structures [4, 5], which exhibit negative stiffness in the vicinity of the unstable equilibrium point. In this case one has to constrain the negative stiffness components in order to ensure that the structure really operates smoothly along the negative branch of the force-displacement graph and does not jump into one of the stable states.

Negative stiffness dampers are already available on the global market. Starting from Platus' patent [6] and related article [7], Minus K Technology [8], founded in 1993 by Dr. Platus, is the leading industry manufacturing negative stiffness dampers. Nevertheless, advantages of such mechanisms were already documented in Russian monograph that was later on translated to English [9]. One of the most recent alternative realizations is given in [10]. In [10] pre-compressed beams represent the negative stiffness component that is stabilized by another spring. The specimen was produced by 3D systems Sinter station Hi Q^{TM} selective laser sintering machine. It was proven that with the increasing pre-compression, implying decrease in fundamental frequency, also the decrease in resonance peak in displacement transmissibility is verified. Nevertheless, it is still a challenging task to design a continuous isotropic three-dimensional material, easy to manufacture, that would globally act in the same way as a discrete mechanism.

In this paper a material produced from polyethylene foam sheets is examined. Such a material is often used for packing protection and it is known for its several other useful properties like easy forming and possibility of heat-welding. In order to integrate an inherent bistable element in such sheets, additional semi-circumferential cuts were introduced. The advantage of this realization is that the material, apart from additional cuts, does not need any special manufacturing technique as the one described in [10]. The base material is easily accessible and cheap. The work presented here is an extension of the preliminary results published in [11], which was developed in continuation with [12].

The new contribution of this paper consists in the innovative realization of a material exhibiting negative stiffness over a range of finite strains and in the development of a method that links this material with a discrete mechanism exploiting also the finite element model. Future work will address its performance optimization.

The paper is organized in the following way. In Section II the polyethylene foam material is described and results of experimental tests are given. In Section III finite element model is developed and numerical results are presented and compared with the experimental testing. A procedure of

linking the continuous model to a discrete mechanism is described in Section IV. New achievements and further challenges are summarized in Section V.

II. POLYETHYLENE FOAM

The polyethylene foam is a cellular material that can be used for packing protection. In the application described in this paper it is utilized as a base material of a periodic arrangement that can exhibit negative stiffness over a certain range of global finite strains. The sheets formed by two light polyethylene foam plates of density 20 $kg \cdot m^{-3}$ glued together were provided by 100metros company [13]. The original sheet size was approximately 260x260x20-23 mm. No information about mechanical properties was supplied by 100metros company. Literature and internet searches on polyethylene foam properties provided large range of material data, but not the mechanical ones. Therefore it was decided to accomplish own tests to estimate the mechanical properties.

Two kinds of specimens were prepared: homogeneous ones for the analysis of the base material properties and specimens with semi-circumferential cuts as a representation of the material with the inherent bistable element (Fig. 1), i.e. of the material exhibiting the negative stiffness. The bistable elements (basic cells) were repeated in one direction to form a periodic material. A simple electric saw was used for straight cuts. Semi-circumferential cuts of 50 mm diameter were added with the help of a heated blade. By simply observing it, it was concluded that the elliptical shape of the bubbles predetermined two directions of orthotropy. The axis of symmetry of the bistable basic cell was aligned with the stiffer direction, that is, the direction of the rising of the foamed cells. Unfortunately, the two plates were not always glued together in the same manner, because such a requirement is not necessary for common applications, and therefore the material testing results showed significant discrepancy.

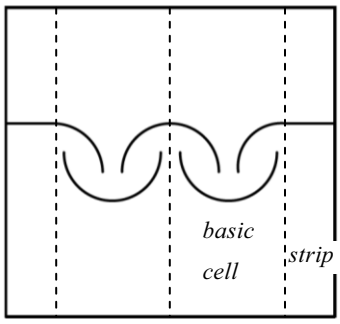

Fig.1. Schematics of the specimen: semi-circular cuts forming the bistable element – two basic cells of the periodic structure with lateral strips

Specimens for uniaxial tension, compression and cyclic loading were prepared at DEC/FCT/UNL (Department of Civil Engineering, Faculdade de Ciências e Technologia, Universidade Nova de Lisboa) and tested at the same place and at DEM/IST/UL (Department of Mechanical Engineering, Instituto Superior Técnico, University of Lisbon). Only the most significant results will be shown. Dimensions of the specimens, results of which are presented, are summarized in Table I.

	Width [mm]	Thickness [mm]	Length [mm]	Uniaxial Test
T01L	37.45	22.78	125	Tension (9mm/min)
T02T	39.92	22.38		
C01L	21.9	38.26	24.46	Compression (3mm/min)
C02T	21.93	38.63	24.45	
C03T	22.1	38.69	24.89	
C04L	25.14	39.1	24.97	
TS01	174	21.39	154	Tension (4mm/min)
TS02	174	21.39	154	Tension (9mm/min)

Table I. Summary of the characteristics of the specimens used in the experimental testing

The notation of the samples is related to the test performed, to the specimen type and to the specimen number. In this sense, first "T" means traction and "C" denotes compression."01" and similar is the sample number. Homogeneous specimens have additional designation: "L" means that the stiffer direction was the longitudinal one, i.e. in the direction of the applied force, and "T" that it was the transversal one, i.e. in the direction perpendicular to the applied force. "S" in used for the specimen with the circumferential cuts.

The specimens were tested on a universal testing machine (model 5566, Instron Corporation Canton, USA) with a load cell of 10 kN. The cross-head velocity was in the range of 3 to 9 $mm \cdot min^{-1}$. The base material is viscoelastic and thus strain rate dependent, hence decrease in stiffness was recorded in higher load rates. Nevertheless, only the tests where the loading was induced in a quasi-static manner, not activating either the viscous behaviour or the inertial properties, are presented here. Results of the tension test on specimens T01L and T02T are shown in Fig.2.

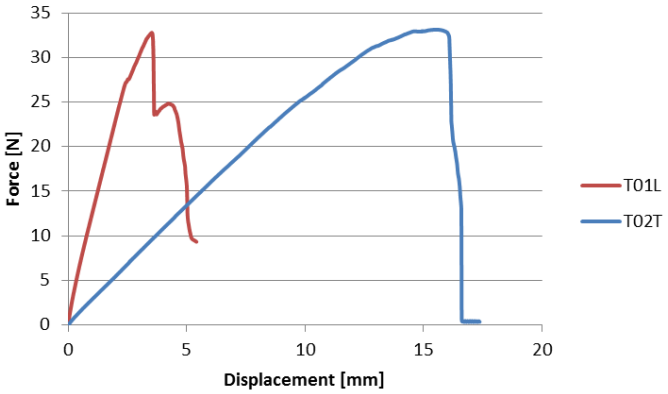

Fig.2. Uniaxial tension of homogeneous specimens

It is necessary to point out that these tests cover very large range of strains and therefore the non-linear behaviour is not clearly visualized in Fig. 2, but there is an initial Young's modulus that is significantly higher than the one fitting the

most of the force-displacement curve. In Fig. 3 secant modulus is plotted in each force increment and overlaid by a trend line obtained by a moving averaging method of rank 4.

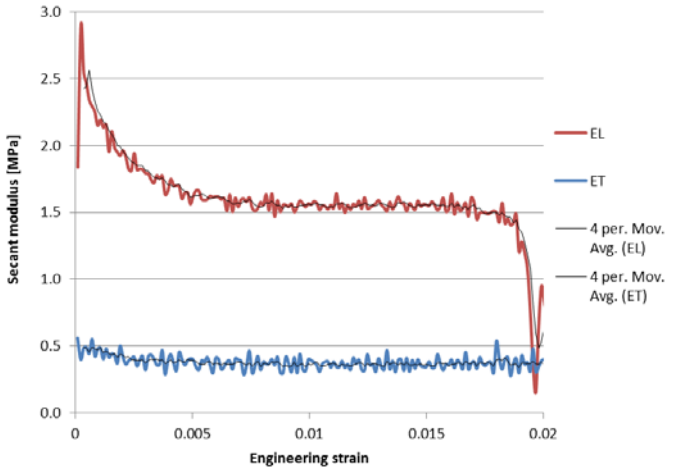

Fig.3. Secant modulus and trend lines obtained by a moving average method related to the initial part of the force-displacement curve from Fig. 2

Regarding the stiffer direction, the elastic modulus decreases exponentially from the initial value of 3 MPa to 1.6 MPa at approximately 0.008 engineering strain and then it drops to 1 MPa at 0.02 engineering strain. Regarding the softer direction, the modulus starts at 0.5 MPa, slowly decreases to 0.4MPa and the specimen is able to bear very large engineering strains, reaching 0.1, when the modulus starts to decrease again. As expected, the behaviour in compression is quite different and the elastic moduli are significantly lower. Experimental curves are shown in Fig. 4.

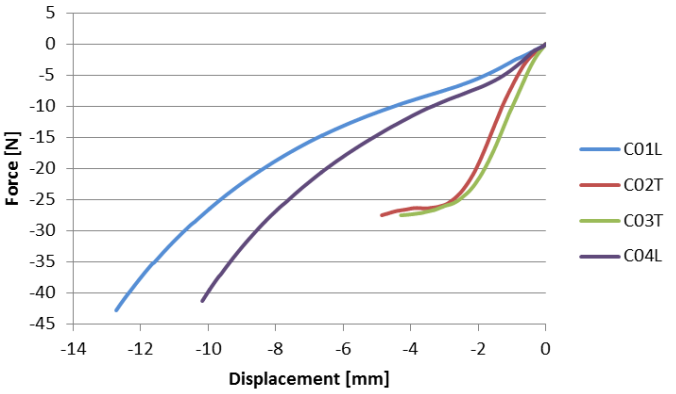

Fig.4. Uniaxial compression of homogeneous specimens

It is seen that for the longitudinal direction the strength is higher in compression than in tension, but the stiffness is significantly lower. There is also a significant difference in longitudinal and transversal directions. Roughly speaking, the stiffness ratio between the stiffer and the softer direction around 4. Moduli in transversal direction do not show significant difference when related to tension and compression, but in longitudinal direction the ratio of tension and compression modulus is around 20.

Furthermore, the bistable structure was tested. As expected, one basic cell of the bistable material was not sufficient to provide the required behaviour, because there was insufficient lateral constraint, and therefore the specimen was unable to show the negative branch in the global stiffness. These results will not be shown here. Specimens with two basic cells and lateral strips (Fig.1.) were tested instead. The lateral strip provided necessary constraint and facilitated a smooth snap through the unstable equilibrium. Two displacement rates were implemented as 4 $mm \cdot min^{-1}$ and 9 $mm \cdot min^{-1}$, but no significant differences were found between the results. Different phases of the loading are shown in Fig. 5, the negative branch is verified between stages (b) and (c).

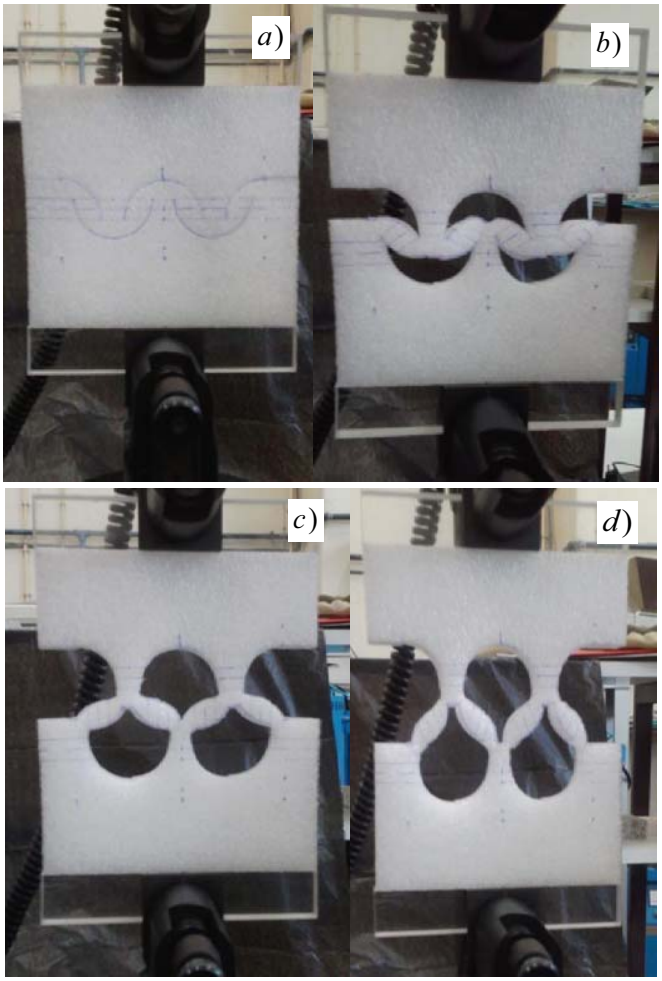

Fig. 5. Tension test on the bistable material: (a) initial position, (b) beginning of the negative stiffness, (c) new beginning of the positive stiffness, (d) initiation of failure

Monotonic displacement-control tests revealed that the negative stiffness region in force-displacement curve is well-formed. However, a visible out-of-plane deformation helped to reach the next stable equilibrium at lower global force, than it would be required by a perfectly plane specimen. Fortunately this fact did not affect the global performance, but in future works some preventive measures have to be taken, like for instance reinforce the specimen by a stiffer thin plate that would prevent out-of plane deformations. The force-

displacement curves related to the experiment described above are shown in Fig. 6.

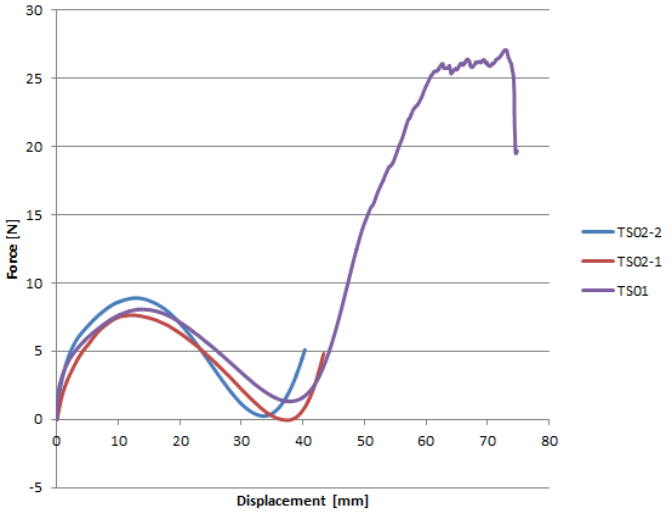

Fig.6. Tension tests on the bistable material

In Fig.6 caption "-1" and "-2" stand for the number of the test performed on the same specimen TS02. Specimen TS01 was left until the failure.

In addition, cyclic tests were performed on the specimen TS02. The objective of the cyclic tests was to show that in displacement control regime the specimen can operate solely over the negative stiffness region. Results are shown in Fig.7.

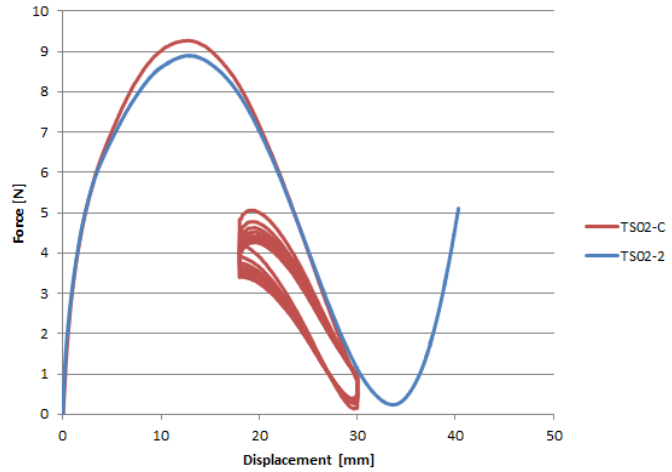

Fig.7. Cyclic test on the bistable material (comparison with the tension test)

Induced displacements in cyclic tests varied between 18 and 30 mm with a short time delay at each extreme position. The gradual displacement increase and decrease had the same duration of 15 s, which was also the time delay at extreme positions. Sharp corners of loading and unloading paths show that during the pause the specimen entered in relaxation, i.e. there is a noticeable decrease in load on the same displacement level in time. Without pausing in the experimental test, the unloading curve would basically follow the same path in each branch because the hysteresis loop is quite narrow. In the legend of Fig.7 "-C" stands for the cyclic test. In Fig. 7 it is also seen that the strain energy is not fully recovered, the main difference being in the first unloading path.

III. FINITE ELEMENT MODEL

The finite element model was created in ANSYS [14] assuming plane stress. Only half of the tested structure was modelled due to the symmetry. The finite element mesh was tested on sensitivity, but relatively fine mesh as shown in Fig. 8 was used, because the calculations were quite fast. A small gap of 0.5 mm was introduced in the cut region to avoid unsuitable element shapes in sharp corners. Regarding the boundary conditions, symmetry condition is used on the left border, the bottom border is fixed in vertical direction and a vertical displacement is imposed on the top. The right border is left fee.

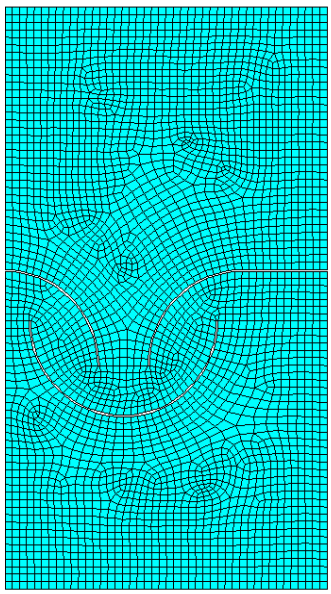

Fig. 8. Finite element mesh in undeformed position

Several material models were tested, starting from the simplest one, the linear elastic material. After several attempts it was concluded that none of the features detected experimentally on homogeneous specimens should be omitted. Thus, the material model must account for orthotropy as well as for elastic non-linearity with different secant moduli in tension and in compression. It was impossible to introduce all these features, because material models available in commercial software like ANSYS and ABAQUS have some limitations.

Hyperelastic models did not perform well, because they usually assume higher stiffness in compression than in tension, but the experimental results obtained here showed the opposite tendency. Main advantage of hyperelastic models was that they did not reveal significant convergence difficulties along the loading path. The disadvantage was that there was no possibility to induce the strong initial non-linearity showed by experimental testing. Hence, the global initial stiffness that

yielded approximately the same maximum force at the onset of the negative branch was significantly lower. The deformation proceeded smoothly without a possibility to create a noticeable "snap-through" effect. The smooth passage over the unstable equilibrium prevented to achieve the zero force level again.

The results presented here were obtained in ANSYS, because in ANSYS it was possible to combine elastic non-linearity (material model MELAS) with orthotropic engineering constants. Unfortunately, this non-linearity is based on von Mises stress-(von Mises total) strain curve and therefore there was no possibility to introduce different tension and compression behaviours. This was the reason, why it was decided to fit the material model to the experimental tests, exploiting some general features obtained experimentally on homogeneous specimens. Regarding the orthotropy, ratio of elastic moduli between the soft and stiff direction was estimated as 4, according to the experimental tests. Since no experiments were performed to estimate other properties, shear modulus was set equal to the soft Young's modulus and Poisson's ratio was estimated. Using APDL (ANSYS Parametric Design Language) an identification optimization module was developed to fit the material data describing the non-linearity to the experimental results.

Non-linear curve was established by a step-by-step procedure, where the slope of the stress-strain curve was tuned to achieve the expected global force, in accordance with the test TS02-2. In this ANSYS material model, none of the posterior slopes can be higher than the initial; also none of them can be negative. The fitting procedure provided sufficient results, but, as expected, sometimes the slope value was not possible to tune, because it affected only a limited region of the finite element model, and therefore it was not sufficient to induce the required changes in the global force.

E_L [MPa]	E_T [MPa]	G_{LT} [MPa]	ν_{LT}
2.25	0.55	0.55	0.3

Table II Engineering constants defining the orthotropy

$\varepsilon_{T,vM}$	σ_{vM} [Pa]	E [MPa]
0	0	2.2
$3.2 \cdot 10^{-04}$	700	0.93
$7.5 \cdot 10^{-04}$	1100	0.39
$1.6 \cdot 10^{-02}$	7000	0.063
0.35	28000	0.034
5.35	200000	0

Table III Values defining the elastic non-linearity

It was concluded that sufficient coincidence with experimental results can be achieved by a material model with orthotropic properties given in Table II and stress-strain curve given in Table III. When confronted with the measured data, it is observed that the initial moduli in Table II are approximately verified by the tension tests on homogeneous specimens. The moduli from Table II decrease proportionally according to Table III (in Table III the values related to the stiffer direction are given) and this decrease is justified by highly compressed localized regions of the model, where compression moduli, i.e. moduli that are much lower, should be used. Thus the corresponding strain where an onset of another slope is specified is lower than the one in Fig. 3. Further decrease in high strains is justified by the non-linearity of the tension as well as compression moduli.

In this way it is possible to fit the material model in a way that main part of the experimental force-displacement curve is the same, the force at the onset of the negative branch achieved experimentally is 8.9 N at 12.6 mm and numerically 8.9 N at 12.5 mm, Fig. 9.

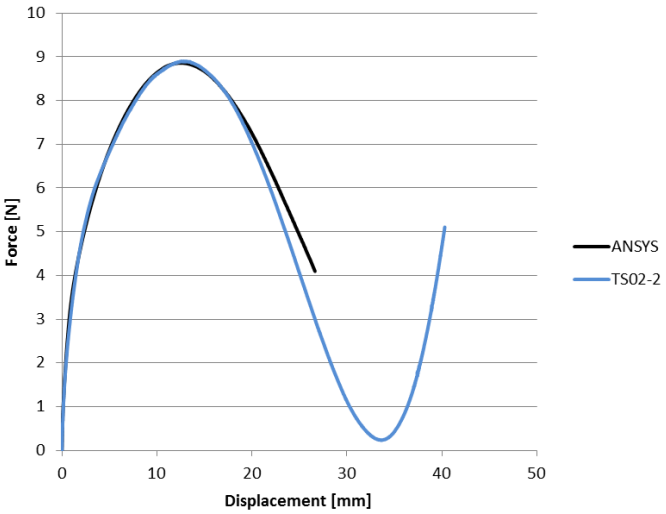

Fig.9. Force-displacement curve: the experimental, ANSYS non-linear elastic material with orthotropic base

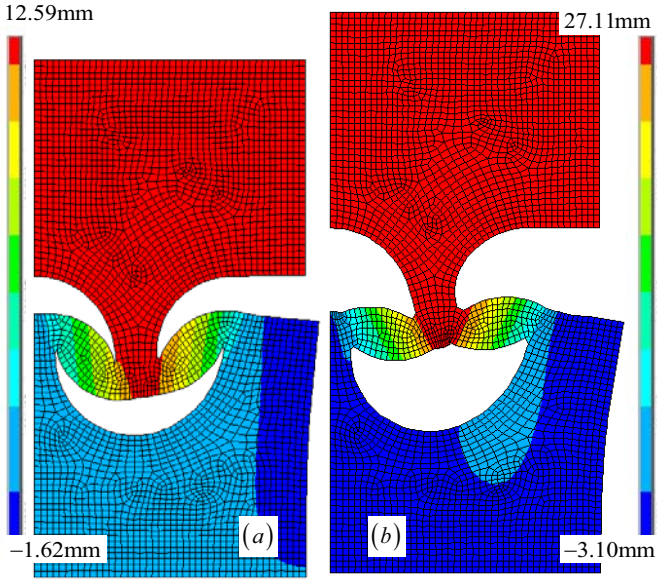

Fig.10. Onset of the negative stiffness (a) and last position (b) determined in ANSYS

In Fig. 10 the distribution of the vertical displacement at the onset of the negative branch and at the final position where

convergence was lost, are shown. Unfortunately, full negative branch was not possible to follow numerically due to convergence difficulties.

This can be explained by the fact that at these stages highly compressed localized regions are present. As the initial part was adjusted to significant tension, it cannot work perfectly well in significant compression, where the material performance should be in general softer. If this additional feature would be possible to introduce, the loading path would have been completed. Also, as written above, during the experimental tests visible out-of-plane deformation occurred and this fact was not modelled numerically. These facts are not related to the finite element mesh. Indeed these limitations come from the material model, and not from the necessity of remeshing as can be seen in Fig. 11 where deformed shapes are obtained for hyperelastic behaviour.

Fig.11. Confirmation of the mesh suitability, hyperelastic (neo-Hookean) behaviour in ANSYS

In summary, it can be concluded that the material identified by the fitting procedure verifies reasonably the data obtained experimentally. It does not work over the full loading path due to software limitations. It would be necessary to introduce a user defined behaviour, which will be accomplished in future work. Hence, the finite element model is ready for shape optimization, because the match with the experimental data is reasonable and very good regarding the initial global stiffness and the maximum force achieved. Future works in this part will avoid three dimensional modelling, because it is preferable to adapt the specimen as already explained.

IV. DISCRETE MECHANISM

The main purpose of this identification is to obtain a model with low computational cost, which can be easily analysed, optimized for dynamic behaviour and provide better insight into physical phenomena involved. The discrete system that is investigated is schematically depicted in Fig. 12. It consists of two pre-compressed spring elements, k_H, a stabilizing spring element, k_V, a viscous damping element, c, and a mass, m. The original length of the horizontal springs is L and the amount of pre-compression is denoted by d. The mechanism is symmetric around the vertical axis. Regarding the dynamic performance two variants of excitation can be considered: (i) kinematic loading, prescribed as time-dependent base excitation, $x_0(t)$, and (ii) force, $F(t)$.

The equation of motion of the one-dimensional system described above reads as:

$$m\ddot{x} + c\left(\dot{x} - \dot{x}_0\right) + F_V = F(t) \tag{1}$$

where the elastic vertical non-linear force F_V is given by

$$F_V = \left(k_V + 2k_H \left(1 - \frac{L}{\sqrt{\left(x - x_0\right)^2 + \left(L - d\right)^2}} \right) \right) \left(x - x_0\right) \tag{2}$$

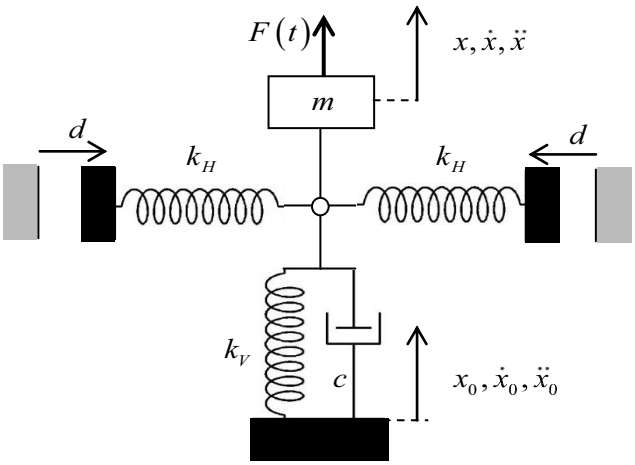

Fig.12. Complete discrete model

Considering only static behaviour and the specimen described and tested in previous sections, then the model can be represented as shown in Fig.13.

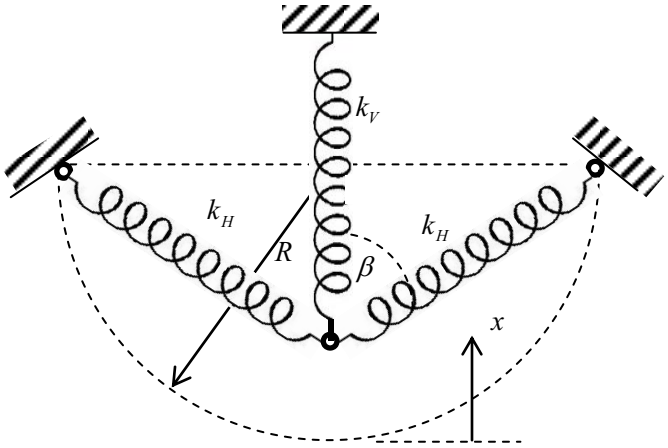

Fig. 13. Spring representation of the tested specimen

In accordance with the experimental tests, it is assumed that the undeformed springs have their free extremities at the position $x = 0$. Other geometrical details are related to the semi-circumferential cuts in the structure. The non-linear force representing the system above can be written as:

$$F_V = k_V x - 2\cos\beta N = k_V x - 2\frac{R-x}{\sqrt{R^2+(R-x)^2}} k_H \left(\sqrt{R^2+(R-x)^2} - R\sqrt{2}\right) = k_V R\xi - 2(1-\xi)k_H R\left(1-\frac{1}{\sqrt{1-\xi+\xi^2/2}}\right) \quad (3)$$

where $\xi = x/R$ and N stands for the elastic force developed in the inclined springs. The objective is to tailor force-displacement curve of this model to be reasonably proximate to the behaviour of the physical model. The parameter connected to the specimen geometry, R, is equal to 25 mm. Consequently, there are only two variables k_V and k_H and 4 essential conditions to fulfil. The essential conditions require placing positions of zero stiffness in terms of the elastic force as well as displacement. The sum of absolute value of these four differences can be taken as the objective function. Optimal parameters, $k_V = 0.18\text{N/mm}$ and $k_H = 1\text{N/mm}$ are obtained by parametric optimization, global performance comparison is shown in Fig. 14.

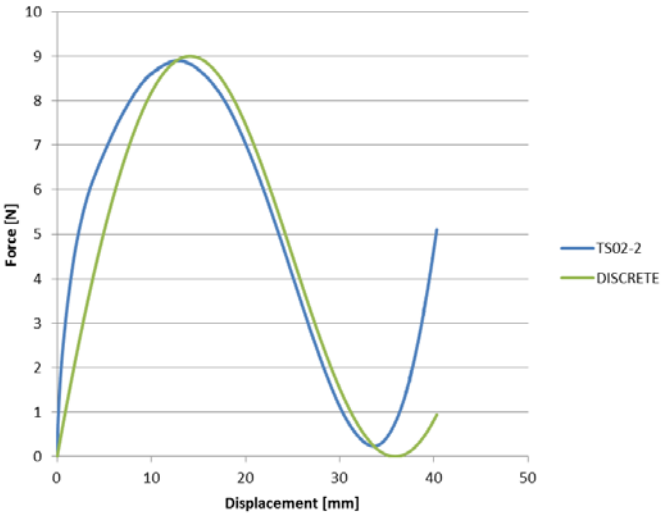

Fig.14. Force-displacement curve: the experimental and the discrete model

As already stated, the discrete model can be easily analysed. Stationary points are determined by:

$$\xi_1 = 1 - \frac{1}{k_V + 2k_H}\sqrt{-(k_V+2k_H)^2 + 2\sqrt[3]{k_H^2(k_V+2k_H)^4}}$$

$$\xi_2 = 1 + \frac{1}{k_V + 2k_H}\sqrt{-(k_V+2k_H)^2 + 2\sqrt[3]{k_H^2(k_V+2k_H)^4}} \quad (4)$$

Under the assumption that

$$8k_H(k_V+2k_H)^2 \geq (k_V+2k_H)^3 \quad (5)$$

Numerical values for optimal parameters are $\xi_1 = 0.573$ and $\xi_2 = 1.427$, that are, as expected, symmetrically placed around value 1. A shift can be introduced as $\tilde{\xi} = \xi - 1$, yielding

$$F_V = k_V R + k_V R\tilde{\xi} + 2\tilde{\xi}k_H R\left(1-\sqrt{\frac{2}{1+\tilde{\xi}^2}}\right) \quad (6)$$

where the first term expresses the pre-compression of the vertical spring. Then the model is equal to the one in Eqs. (1-2). Detailed analysis of this model is presented in [10].

V. Conclusions

A bistable nonlinear material that exhibits negative stiffness over a finite range of global strain was analysed experimentally and numerically. Correspondence with a finite element model and a discrete model was established. For the discrete model standard methods of analysis can be utilized. In future works the discrete model will be optimized for vibration damping. Shape optimization of semi-circumferential cuts will be performed on the finite element model and conclusions will be tested experimentally.

Acknowledgment

The authors would like to express their gratitude to 100metros company for providing the polyethylene sheets. They also greatly appreciate the help of Ph.D. students at FCT/UNL, especially of MSc. Hugo Fernandes and support to experimental testing given by Ph.D. student at IST/UL MSc. Ana Catarina Vale under supervision of Prof.ª Fátima Vaz (IST/UL).

References

[1] T. Jaglinski, D. Kochmann, D. Stone, and R.S. Lakes, "Materials with Viscoelastic Stiffness Greater than Diamond," *Science*, vol. 315, pp. 620-622, Feb. 2007.

[2] R.S. Lakes, "Extreme Damping in Composite Materials with a Negative Stiffness Phase," *Phys. Rev. Lett.,* vol. 86(13), pp. 2897-2900, 2001.

[3] J. Prasad, and A.R. Diaz, "Viscoelastic Material Design with Negative Stiffness Components using Topology Optimization," *Struct. Multidisciplinary Optimizat.*, vol. 38, pp. 583 –597, 2009

[4] R.S. Lakes, "Extreme Damping in Compliant Composites with a Negative-Stiffness Phase," *Phil. Mag. Lett.*, vol. 81(2), pp. 95–100, 2001.

[5] H. Kalathur, and R.S. Lakes, "Column Dampers with Negative Stiffness: High Damping at Small Amplitude," *Smart Mater. Struct.*, vol. 22(8), 084013-21, 2013.

[6] D.L. Platus, "Vibration Isolation System," WIPO Patent Application WO/1991/002921, 1991.

[7] D.L. Platus, "Smoothing out Bad Vibes," *Mach. Des.*, vol. 26, pp. 123-130, 1993.

[8] http://www.minusk.com/index.html

[9] P. Alabuzhev, A. Gritchin, L. Kim, G. Migirenko, V. Chon, and P. Stepanov, *Vibration Protecting and Measuring Systems with Quasi-Zero Stiffness*. Hemisphere Publishing Corporation, 1989 (published in Russian in 1986).

[10] L. Kashdan, C.C. Seepersad, M. Haberman, and P.S. Wilson, "Design, fabrication, and evaluation of negative stiffness elements using SLS," *Rapid Prototyping J.*, vol. 18(3), pp. 194 – 200, 2012.

[11] J. Heczko, Z. Dimitrovová, and H.C. Rodrigues, "Composite material with negative stiffness inclusion for vibration damping: The effect of a nonlinear bistable element," in *Proc. 11th Int. Conf. on Vibration Problems (ICOVP-2013)*, Lisbon, Portugal, 9-12 September 2013.

[12] J. Heczko, Z. Dimitrovová, and H.C. Rodrigues, "Optimization of linear and non-linear one-dimensional visco-elastic isolators for passive vibration control," in *Proc. 2nd Int. Conf. on Eng. Optimizat. (EngOpt2010)*, Lisbon, Portugal, 6-9 September 2010.

[13] www.**100metros**.pt/

[14] Release 12.1 Documentation for ANSYS, Swanson Analysis Systems IP, Inc., 2009.